

Article

Fast Ion Speed Diffusion Effect on Distributions of Fusion Neutrons

Pavel Goncharov 

Advanced Plasma Research Laboratory, Peter the Great St. Petersburg Polytechnic University,
195251 Saint Petersburg, Russia; p.goncharov@spbstu.ru

Featured Application: Numerical modelling of yields and distributions of nuclear fusion products in magnetically confined plasma.

Abstract: Velocity distributions of fuel nuclei enter the formulae for distributions of products of fusion reactions in plasma. The formulae contain multiple integration, which is a computationally heavy task. Therefore, simplifications of the integrand are advantageous. One of possible simplifications is the use of closed-form analytical distributions of fast deuterons and tritons, accounting for slowing down and pitch-angle scattering and neglecting the speed diffusion. The plausibility of such a model has been studied from the viewpoint of its influence on the calculated spectra of fusion neutrons. Calculations have shown that the speed diffusion effect on suprathermal ion distribution tails does not significantly alter the qualitative behaviour of energy and angle distributions of fusion products in a beam-heated plasma.

Keywords: neutron spectra; suprathermal ions; speed diffusion



Citation: Goncharov, P. Fast Ion Speed Diffusion Effect on Distributions of Fusion Neutrons. *Appl. Sci.* **2023**, *13*, 1701. <https://doi.org/10.3390/app13031701>

Academic Editor: Arkady Serikov

Received: 6 January 2023

Revised: 20 January 2023

Accepted: 24 January 2023

Published: 29 January 2023



Copyright: © 2023 by the author. Licensee MDPI, Basel, Switzerland. This article is an open access article distributed under the terms and conditions of the Creative Commons Attribution (CC BY) license (<https://creativecommons.org/licenses/by/4.0/>).

1. Introduction

Research and development activities on fusion neutron sources for fundamental science and technological applications are being pursued by universities, laboratories, and other organizations in various countries of the world, as indicated in [1–6] and the references therein. An analysis of possibilities of constructing fusion neutron sources based on tokamaks, stellarators, and laser systems was recently published in [1]. In [2,3], the long-standing concept of using controlled nuclear fusion systems as neutron sources was considered in light of the developments of the past decade. In [4–11], the main attention was paid to tokamaks. In particular, in [4] and [5], neutron sources based on spherical and classical tokamaks, respectively, were investigated. Article [6] is dedicated to the analysis of the economic feasibility of tokamaks with conventional and superconducting windings as neutron sources applied to the transmutation of transuranium elements. Fusion neutron sources using deuterium–deuterium and deuterium–tritium reactions in a tokamak were considered in [7] and [8], respectively. In [9], an integral approach was applied to the modelling of a plasma neutron source based on a classical tokamak. Article [10] is devoted to a similar range of issues for a spherical tokamak. A three-dimensional model developed as part of the demonstration fusion neutron source DEMO-FNS project for neutronics calculations by Monte Carlo methods was presented in [11].

The yield and energy spectrum of neutrons belong to the main characteristics of the source. Along with conceptual and engineering design studies of fusion neutron sources employing magnetically confined plasma, calculations of energetic and angular distributions of fusion neutrons are essential for neutron spectroscopy [12], and for fast particle physics in plasma [13,14], as well as for estimating loads on the first walls of reactors due to fluxes of neutrons and other fast particles [15]. Modelling of tritium breeding, subcritical fission, transmutation, and other purpose blankets also requires the knowledge of spectra of incident fusion neutrons [15–18].

Reviews [19,20] consider the stages of development and prospects of fusion–fission hybrid systems and emphasize the important role of the coefficient that takes into account the increased production of neutrons in subcritical systems in the initial generations of fission chain reactions. The value of this coefficient in the formula for the number of fission neutrons per one fusion neutron can exceed two. Energies of neutrons produced in the deuterium–tritium fusion reaction are much higher than the average fission neutron energy. In this regard, the energy spectrum of a fusion neutron source strongly manifests itself in the initial generations of subcritical fission.

As a rule, in research and development works on controlled nuclear fusion in toroidal magnetic configurations, calculations of distributions of a plasma neutron source are combined with numerical modelling of the penetration of fast neutral beams into the plasma, with calculations of distributions of plasma ion velocities, simulations of neutron transport processes, and need to be included in more extensive integrated modelling. Studies [21] and [22] are devoted to the analysis of possible ranges of parameters of tokamak neutron sources with neutral beam-heated plasmas, and the examination of neutral beam-driven plasma operation scenarios of fusion neutron sources.

In magnetic plasma confinement devices, the anisotropy of fuel nuclei velocity distributions due to beam and wave heating leads to anisotropy of neutron energy spectra. An approach to calculating energy spectra of fusion neutrons, based on the use of Monte Carlo methods, exists, for example in [23,24], and an approach based on the explicit analytical formulae obtained in [25–27].

From the point of view of the development of the physics basis, as well as the reliability and the computational speed of integrated modelling, the use of analytical results is beneficial. The formulae for distributions of fusion products found in [25] themselves are general, i.e., suitable for arbitrary distributions of velocities of fuel nuclei. Either distributions obtained experimentally can be plugged in, or those calculated numerically. In [25], a compact simplified analytical model of anisotropic fast ion distributions neglecting the speed diffusion effect on high-energy tails was applied as a sample case, which is convenient, being expressed in a closed form. The purpose of this work was to figure out to what extent such a simplification is plausible. The overall population of energetic particles strongly influences the neutron production [22]. Both in the DEMO-FNS classical tokamak [5] and in the FNS-ST spherical tokamak [4], contributions of beam–plasma interactions to the total fusion rates are either on par with or exceed thermonuclear rates, i.e., contributions of Maxwellian populations of fuel nuclei. It is therefore preferable to evaluate the sensitivity of neutron spectra to modifications of high energy ion distribution tails caused by speed diffusion. Section 2 describes the mathematical models used for this purpose, and Section 3 presents the results, followed by a summary given in Section 4.

2. Modelling Techniques

At an early stage of nuclear fusion research, possible approaches to calculating the distributions of fusion neutrons were discussed in [28], where deuterium–deuterium fusion reactions were considered and the formula for the fusion neutron spectrum was given for the case when the interacting fuel nuclei are identical and their distributions are Maxwellian, without taking into account the anisotropy of the differential cross section. Some other special cases were also considered, namely, for the generalized Maxwellian distribution with different values of perpendicular and parallel temperatures and for monoenergetic distributions. According to the available data for the ${}^3\text{H}({}^2\text{H},\text{n}){}^4\text{He}$ reaction, the differential cross-section exhibits a rather weak angular dependence over a wide energy range, whereas for the ${}^2\text{H}({}^2\text{H},\text{n}){}^3\text{He}$ reaction, the anisotropy of the differential cross-section is quite distinct. For some particular cases, a simplified angular dependence of the differential cross-section of the deuterium–deuterium fusion reaction was assumed in [28].

Later, in [29], a method to calculate the energy spectra of neutrons was proposed, based on chain rule differentiation of the total cross-section with respect to the emission angle cosine, which, in turn, is related to the kinetic energy of the neutron owing to

energy and momentum conservation. Estimations of fusion neutron spectra in a beam-Maxwellian plasma reported in [30] were based on [28,29]. Suprathermal ions, other than those injected by heating beams, may influence the neutron spectra, e.g., so-called knocked-on deuterons and tritons formed due to close elastic collisions with fusion-born α -particles, as discussed in [31,32]. Neutron spectra obtained using Monte Carlo modelling techniques were described in [33], and afterwards in other studies of magnetic and inertial confinement fusion, such as [34,35]. For a number of particular cases, analytical expressions were considered, such as [36,37]. However, the mentioned publications [28–37] do not contain general formulae.

For the purpose of clarifying the effect of the speed diffusion of fast ions on neutron spectra, straightforward analytical results of a general form for double differential fusion reactivities $\frac{d^2 R_{12}}{dE_3 d\Omega_3}$ with respect to neutron energy and laboratory emission angle obtained in [25] have been used in this work. For reactions between two colliding fuel nuclei (species “1” and “2”) and two product particles (species “3” and “4”), the general methods in [25] are called the S- and the L-algorithms, enabling calculations of distributions of fusion products for arbitrary anisotropic distributions of fuel nuclei velocities, also taking into account the angular anisotropy of differential cross-sections of fusion reactions. Either of these equivalent methods are suitable. Species “3” means neutrons herein. Although the S- and the L-algorithm differ mathematically, both are 5-fold integrals essentially based on the use of the relation

$$(\mathbf{v}_3 - \mathbf{V})^2 = \frac{2m_4}{Mm_3} \left(\frac{\mu v^2}{2} + q_f \right) \tag{1}$$

following from the energy and momentum conservation laws with M and μ being the sum of the fuel particle masses m_1 and m_2 and their reduced mass, respectively, \mathbf{v}_3 being the laboratory velocity of product “3”, \mathbf{V} being the centre of mass velocity, v designating the relative velocity of the fuel particles, and q_f being the energy released in an elementary fusion reaction due to the mass defect. Up-to-date values of particle masses can be found in [38].

Anisotropic distributions of fuel nuclei velocities in fusion plasma subject to neutral beam injection or radiofrequency heating were described, for example, in [39] and the references therein. This anisotropy, in turn, leads to an anisotropy of the distributions of nuclear fusion products. Modified S- and L-algorithms were published in [27] on the basis of the same geometric technique as in [26]. This method still retains the generality of [25]. Detailed descriptions of the computations of neutron spectra are explained in the corresponding references.

The compact analytical anisotropic model, used in [25] as a sample case of fuel nuclei velocity distributions, that does not take into account the speed diffusion effect, is as follows:

$$f_{1,2}(\mathbf{v}, \vartheta) = (1 - A_{1,2}) f_{1,2}^{(M)}(\mathbf{v}) + A_{1,2} \sum_{n=0}^{\infty} \phi_n^{(1,2)}(\mathbf{v}) P_n(\cos \vartheta) \tag{2}$$

where the second term describes populations of suprathermal particles of species “1” and “2” with energetic tail fractions $0 \leq A_{1,2} \leq 1$, the term

$$f_{1,2}^{(M)}(\mathbf{v}_{1,2}) = \frac{1}{\pi^{3/2}} \left(\frac{m_{1,2}}{2T_{1,2}} \right)^{3/2} \exp \left(-\frac{m_{1,2} v_{1,2}^2}{2T_{1,2}} \right) \tag{3}$$

is the Maxwellian distribution of bulk thermalized particles, $P_n(\cos \vartheta)$ are Legendre polynomials,

$$\phi_n^{(1,2)}(\mathbf{v}) = \frac{\kappa_{1,2} Z_{1,2}^{(b)}}{V_c^3} (2n + 1) Z_n^{(1,2)} \frac{H(\mathbf{v}_{inj1,2} - \mathbf{v})}{b_{1,2}(\mathbf{v})} e^{-\frac{n(n+1)}{\varepsilon_{1,2} v T_e} \int_{\mathbf{v}}^{\mathbf{v}_{inj1,2}} \frac{c_{1,2}(\bar{\mathbf{v}})}{b_{1,2}(\bar{\mathbf{v}})} d\bar{\mathbf{v}}} \tag{4}$$

Dimensionless functions $b_{1,2}(v)$ and $c_{1,2}(v)$ in (4) are given by

$$b_{1,2}(v) = Z_{1,2}^{(b)} \left(1 + \frac{v^3}{V_{c1,2}^3} \right) \tag{5}$$

$$c_{1,2}(v) = \frac{\varepsilon_{1,2} Z^{(eff)}}{2} \frac{v_{Te}}{v} + \frac{2\varepsilon_{1,2}}{3\sqrt{\pi}} \tag{6}$$

where

$$Z^{(eff)} = \frac{1}{n_e} \sum_{i=1}^{N_i} n_i Z_i^2 \tag{7}$$

The value

$$V_{c1,2} = \left(\frac{3\sqrt{\pi}}{4} Z_{1,2}^{(b)} \right)^{1/3} \varepsilon_{1,2} v_{Te} \tag{8}$$

referred to as critical velocity is proportional to the electron thermal velocity $v_{Te} = \sqrt{2T_e/m_e}$ determined by the electron temperature T_e . The parameters in (8) are dimensionless quantities given by

$$\varepsilon_{1,2} = \left(\frac{m_e}{m_{1,2}} \right)^{1/3} \tag{9}$$

$$Z_{1,2}^{(b)} = \frac{m_{1,2}}{n_e} \sum_{i=1}^N \frac{n_i Z_i^2}{m_i} \tag{10}$$

where m_e is the electron mass, n_e is the electron density, the summation is over the N species of the background plasma ions with masses m_i , electric charge numbers Z_i and densities n_i . The values

$$\kappa_{1,2} = \left(\frac{4\pi}{3} \ln \left(1 + \frac{v_{inj1,2}^3}{V_{c1,2}^3} \right) \right)^{-1} \tag{11}$$

are normalizing constants. Finally, coefficients

$$\mathcal{Z}_n^{(1,2)} = \int_0^\pi \mathcal{Z}_{1,2}(\vartheta) P_n(\cos \vartheta) \sin \vartheta d\vartheta \tag{12}$$

are dimensionless quantities determined by the unity-normalized angular dependence factor $\mathcal{Z}_{1,2}(\vartheta)$ of the monoenergetic fast particle source in the plasma, $H(v_{inj1,2} - v)$ is the unit step function, and $v_{inj1,2}$ are the injection velocities of fast particles.

The model used here to take into account the speed diffusion effect is based on numerical solutions of the Landau–Boltzmann kinetic equation for the distribution functions of fuel nuclei $n_{1,2}(\mathbf{r})f_{1,2}(\mathbf{v})$ [cm^{-6}s^3]

$$\frac{\partial(n_{1,2}f_{1,2})}{\partial t} = C_{1,2} + S_{1,2} - \frac{n_{1,2}f_{1,2}}{\tau_{1,2}} \tag{13}$$

where $S_{1,2}$ is the monoenergetic fast particle source

$$S_{1,2}(v, \vartheta) = \frac{S_{1,2}^{inj}}{2\pi v^2} \delta(v - v_{inj1,2}) \mathcal{Z}_{1,2}(\vartheta) \tag{14}$$

with $\delta(v - v_{inj1,2})$ being the Dirac delta function and $S_{1,2}^{inj}$ [$\text{cm}^{-3}\text{s}^{-1}$] being the source rate, i.e., the number of injected particles of species “1” or “2” per unit volume per unit time. Fast particle lifetime is denoted by $\tau_{1,2}$ to enable a simple simulation of losses.

Maxwellian background plasma is assumed, and the Landau collision term for fast ion species “1” or “2” is

$$C_{1,2} = \frac{v_{c1,2}^3}{\tau_{s1,2}} \frac{1}{v^2} \left(\frac{\partial}{\partial v} \left(v_{c1,2}^2 \frac{a_{1,2}(v)}{2v} \frac{\partial(n_{1,2}f_{1,2})}{\partial v} + b_{1,2}(v)(n_{1,2}f_{1,2}) \right) + \frac{c_{1,2}(v)}{v_{c1,2}} \frac{1}{\sin \vartheta} \frac{\partial}{\partial \vartheta} \left(\sin \vartheta \frac{\partial(n_{1,2}f_{1,2})}{\partial \vartheta} \right) \right) \tag{15}$$

where

$$v_{c1,2} = \varepsilon_{1,2} v T_e \tag{16}$$

and

$$\tau_{s1,2} = \left(\frac{m_{1,2}}{Z_{1,2} e \omega_{pe}} \right)^2 \frac{v_{c1,2}^3}{\Lambda m_e} \tag{17}$$

with $Z_{1,2}$ being the electric charge numbers of the injected particles, Λ being the Coulomb logarithm, and

$$\omega_{pe} = \sqrt{\frac{4\pi n_e e^2}{m_e}} \tag{18}$$

being the electron plasma frequency with e designating the elementary charge.

The terms containing $a_{1,2}(v)$ and $c_{1,2}(v)$ are associated with the diffusion tensor in velocity space. These terms are responsible for the speed diffusion and pitch angle scattering, respectively. The term with $b_{1,2}(v)$ is associated with the dynamic friction force and describes the slowing-down process. Expressions (5) and (6) given above are simplified. Complete formulae for $a_{1,2}(v)$, $b_{1,2}(v)$, and $c_{1,2}(v)$ are given in [39], as well as the details of obtaining numerical steady state solutions of (13).

It is worth mentioning that an analytical approach is also possible. In brief, for an isotropic case, such an approach can be described as follows. The steady state implies zero time derivative in Equation (13). The isotropy implies no angular dependence, i.e., zero angular derivative in the term with $c_{1,2}(v)$. Neglecting the speed diffusion, i.e., neglecting the term with $a_{1,2}(v)$ bearing in mind the small parameter $\varepsilon_{1,2}$, and assuming an infinite $\tau_{1,2}$, i.e., no losses of particles for simplicity, a steady state isotropic solution of (13) can be readily obtained in the form of the so-called classical slowing-down distribution

$$n_{1,2}f_{1,2}(v) = \frac{S_{1,2}^{inj} \tau_{s1,2}}{4\pi v_{c1,2}^3} \frac{1}{b_{1,2}(v)} H(v_{inj1,2} - v) \tag{19}$$

where the unit step function is obviously cutting off the distribution tail above $v_{inj1,2}$. The most straightforward way to obtain a more sophisticated analytical solution taking into account the speed diffusion can be demonstrated for the case when all background plasma species are in thermal equilibrium with equal temperatures T . Since the collision term nullifies in thermal equilibrium, the Maxwellian distribution function $\exp(-m_{1,2}v^2/2T)$ is to be a partial solution of the homogeneous differential equation corresponding to (13). Next, the second independent partial solution of the homogeneous equation can be found, and afterwards the general analytical solution of Equation (13) as explained in [39]. However, numerical solutions are used herein for the designated purposes of studying the effect on the resultant fusion neutron spectra.

3. Calculation Results

To study the influence of the speed diffusion effect on distributions of emission energies and angles of nuclear fusion products, calculations of energy spectra of neutrons produced in a candidate operating regime of FNS-ST [4] in $^3\text{H}(^2\text{H},n)^4\text{He}$ and $^2\text{H}(^2\text{H},n)^3\text{He}$ reactions were performed using the simple analytical anisotropic model (2) similarly to [25], as well as using steady-state numerical solutions of (13) where the speed diffusion effect is included. Parameterisations of differential cross-sections from [40] and [41] were used. Numerical

solutions of the Landau–Boltzmann kinetic Equation (13) were obtained using [39]. The beam and plasma parameters of the FNS-ST candidate operating regime, used herein as a sample case, are similar to those used in simulations reported in [42].

In the modelling of the ${}^3\text{H}({}^2\text{H},n){}^4\text{He}$ reaction, mono-directional injection of monoenergetic deuterons and tritons into Maxwellian deuterium–tritium background plasma was assumed. The injection energy 130 keV, equal electron and ion temperatures 7 keV, and the electron density $n_e = 10^{14} \text{ cm}^{-3}$ were taken as input values. Such are the FNS-ST core plasma parameters adopted in [42]. The injection angle value, i.e., the pitch angle of particles injected by the source, was 30° , in other words, the angular dependence factor $\mathcal{Z}_{1,2}(\vartheta)$ in (12) and (14) was taken in the form a delta-like peak at the injection angle. In fact, the source function of fast ions originating from neutral beam injection into a toroidal magnetically confined plasma is characterized by a certain angular distribution, rather than a particular injection angle as explained in [43]; however, a narrow distribution around the selected injection angle value was assumed here for simplicity. The fraction of suprathermal tail particles $A_{1,2}$ in (2) was 2.5%.

Figure 1a,b show surface plots of anisotropic distributions of deuteron velocities and triton velocities, correspondingly, calculated for the same conditions. The results of simplified calculations using Formula (2), not taking into account the speed diffusion, are depicted by darker colours, whereas the surfaces depicted by semi-transparent lighter colours refer to the solutions of Equation (13) with the speed diffusion effect. The presence of high-energy tails in the vicinity of the injection angle can be seen. The unit step function in Formula (4) is cutting off these tails above the injection velocities, as the darker surfaces illustrate. The lighter surfaces exhibit the tails extending to the regions above the injection velocities that are different for deuterons and tritons due to the difference of masses.

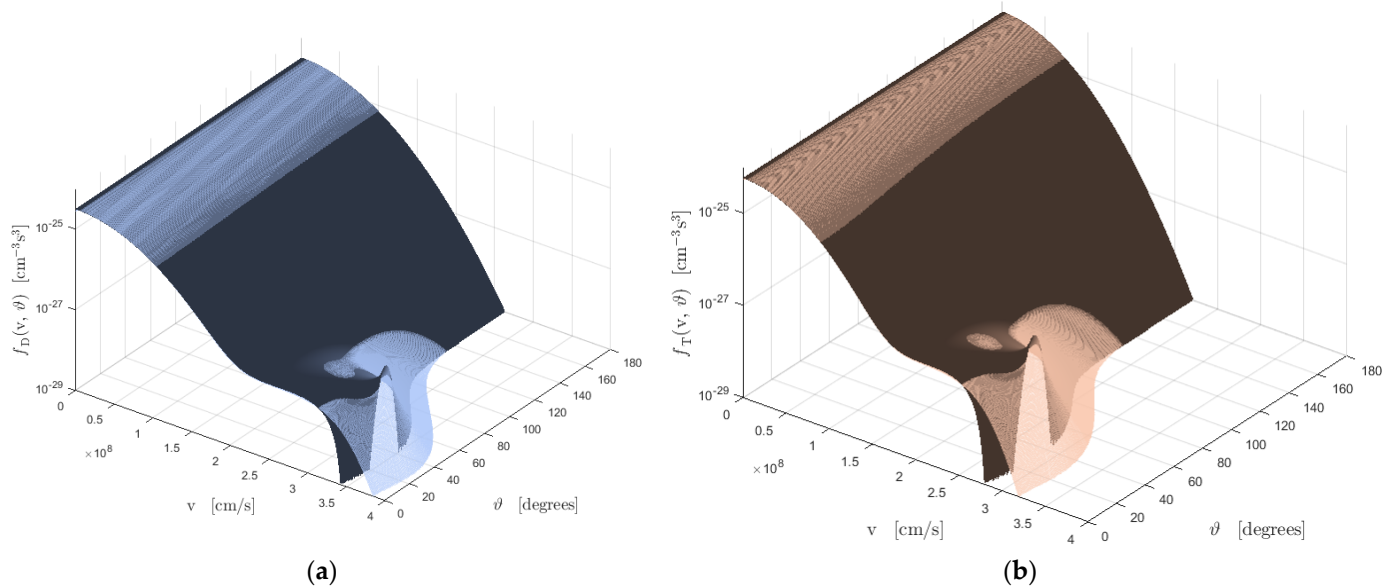


Figure 1. Surface plots of anisotropic distributions of fuel nuclei for the case of injection energy 130 keV, suprathermal fraction 2.5%, and injection angle 30° without taking into account the speed diffusion (darker colours) and with the speed diffusion taken into account (lighter colours). (a) Deuteron velocity distribution functions; (b) triton velocity distribution functions.

Figure 2 shows contour plots of the same distributions of deuteron velocities and triton velocities as shown in Figure 1. The axes are the parallel and perpendicular projections of velocity $v_{\parallel} = v \cos \vartheta$ and $v_{\perp} = v \sin \vartheta$. Model (2) is shown by dashed lines and model (13) is shown by solid lines. Contour lines of low-energy parts of distributions of thermalized particles are circular. The anisotropy of velocity distributions of high-energy particles can be seen as distortions of contour lines in the vicinity of the injection velocity and injection angle.

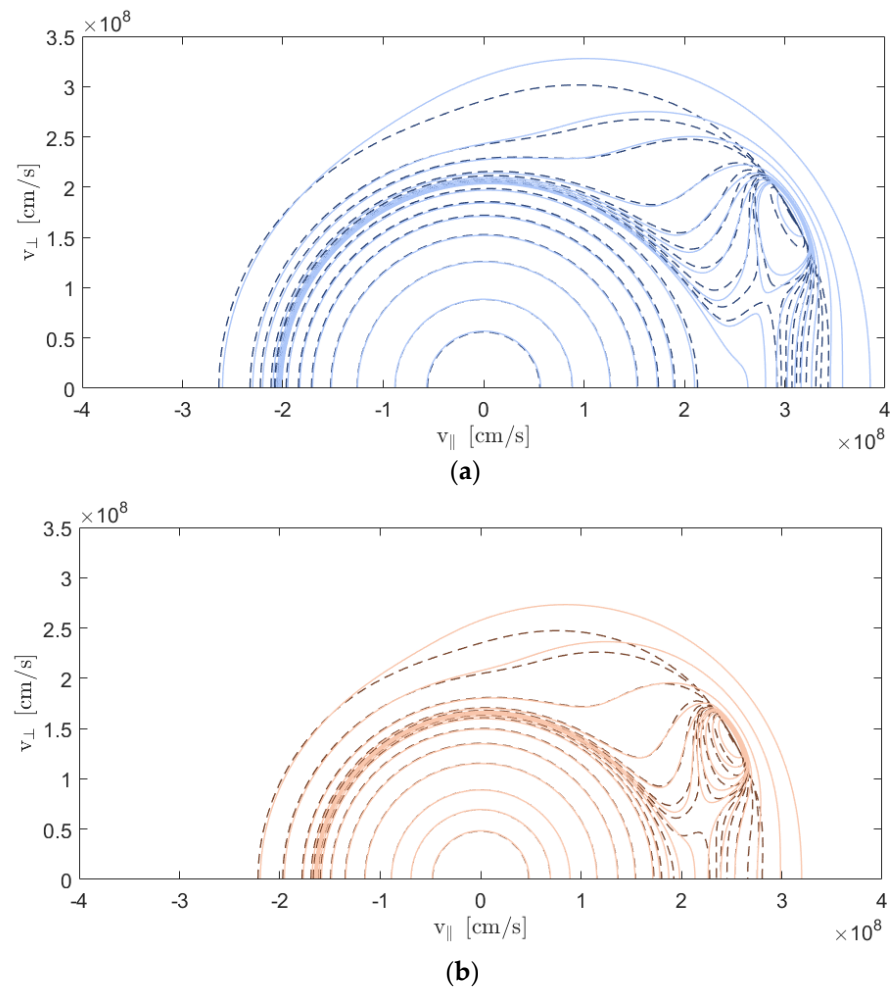


Figure 2. Contour plots of the anisotropic distributions of fuel nuclei shown in Figure 1 without the speed diffusion (dashed lines) and with the speed diffusion (solid lines). (a) Deuteron velocity distribution functions; (b) triton velocity distribution functions.

It should be noted that the speed diffusion is responsible for thermalization of injected fast ions governed by Equation (13). The Maxwellian term was introduced artificially in model (2) to describe the bulk plasma ion population. Therefore, the low-energy parts of darker and lighter surfaces in Figure 1 coincide as well as the low-energy contours shown by dashed and solid lines in Figure 2.

Modelling of the ${}^2\text{H}({}^2\text{H},n){}^3\text{He}$ reaction was performed assuming mono-directional injection of monoenergetic 130 keV deuterons into Maxwellian deuterium target plasma, with equal electron and ion temperatures 7 keV and the electron density $n_e = 10^{14} \text{ cm}^{-3}$. The injection angle 90° was used as a sample case, and the fraction of suprathermal tail deuterons was 2.5%.

Figure 3a shows 3D plots of two anisotropic distributions of velocities of deuterium nuclei calculated for the same conditions. The dark-blue surface corresponds to the simplified model (2) without taking into account the speed diffusion. The light-blue surface corresponds to the semianalytical model based on (13), taking into account the speed diffusion effect. The presence of a high-energy tail in the vicinity of the injection angle can be seen. The tail is extending for the light-blue surface further than for the dark-blue surface. Figure 3b illustrates these same deuteron velocity distributions as 2D plots for three selected pitch angles: 30° , 60° , and 90° .

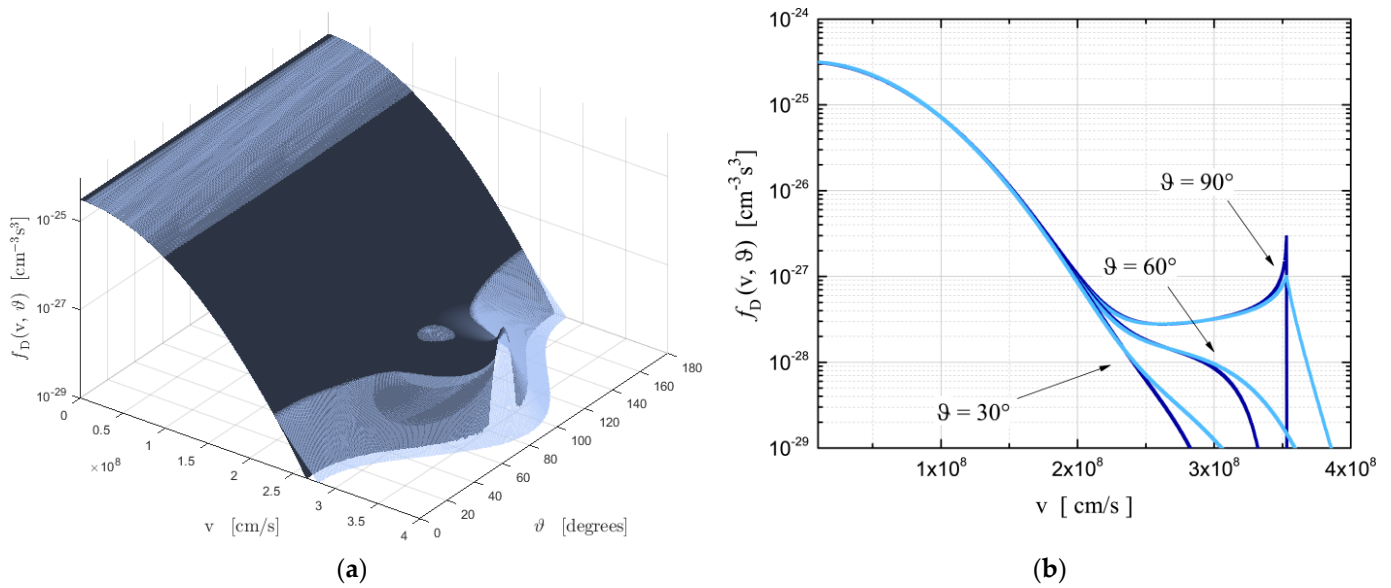


Figure 3. Anisotropic distributions of deuterons without taking into account the speed diffusion (dark blue) and with the speed diffusion taken into account (light blue) for the case of injection energy 130 keV, suprathermal fraction 2.5%, and injection angle 90° , depicted as: (a) surface plots; (b) velocity distribution functions of deuterons with pitch angles 30° , 60° , and 90° .

Double differential reactivities with respect to neutron energy E_n and laboratory emission angle ϑ_n are shown as surface plots in Figure 4a,b for $^3\text{H}(^2\text{H},n)^4\text{He}$ reactions and for $^2\text{H}(^2\text{H},n)^3\text{He}$ reactions, correspondingly. Blue surfaces show the results obtained with the fast ion speed diffusion effect and grey surfaces show the results obtained without the fast ion speed diffusion effect. The presence of extra tails of suprathermal ions with somewhat higher energies in the former case is responsible for a slight increase in the reactivities; however, the shapes of the surfaces do not significantly differ, qualitatively.

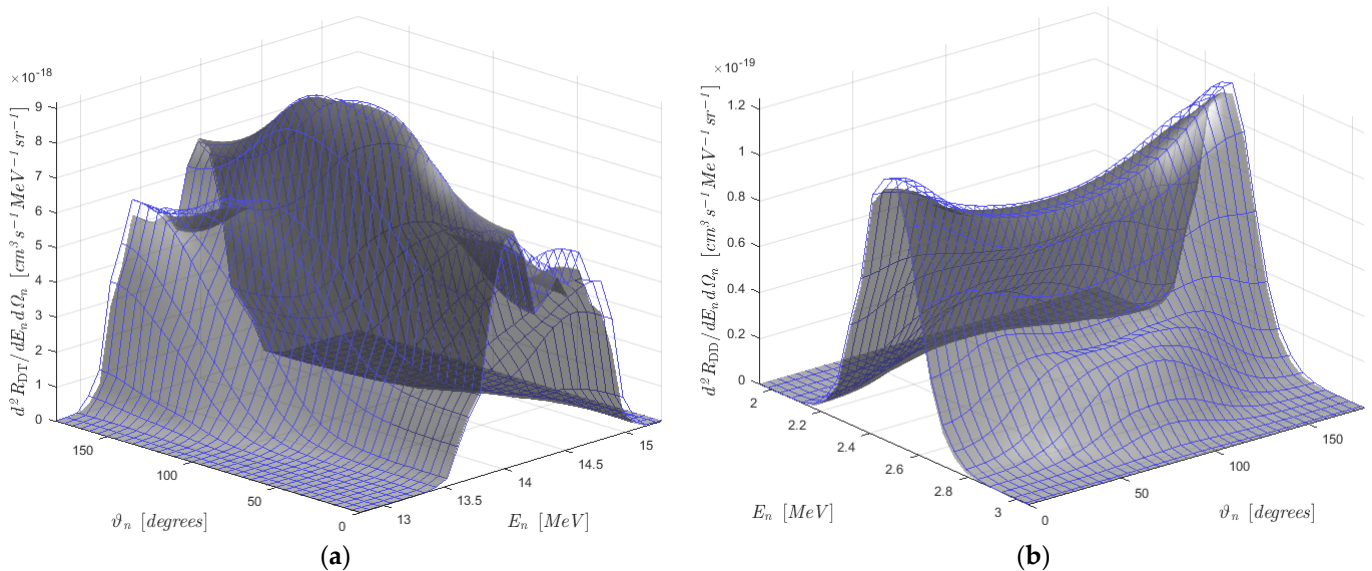


Figure 4. Energetic and angular distributions of fusion neutrons calculated with fast ion speed diffusion effect (blue surfaces) and without fast ion speed diffusion effect (grey surfaces). (a) For $^3\text{H}(^2\text{H},n)^4\text{He}$ reactions corresponding to velocity distributions of deuterons and tritons shown in Figures 1 and 2; (b) for $^2\text{H}(^2\text{H},n)^3\text{He}$ reactions corresponding to velocity distributions of deuterons shown in Figure 3.

For clarity, the difference between the neutron distributions obtained with and without the effect of speed diffusion of fast deuterium and tritium ions is shown in Figure 5a for the ${}^3\text{H}({}^2\text{H},n){}^4\text{He}$ reaction and in Figure 5b the ${}^2\text{H}({}^2\text{H},n){}^3\text{He}$ reaction.

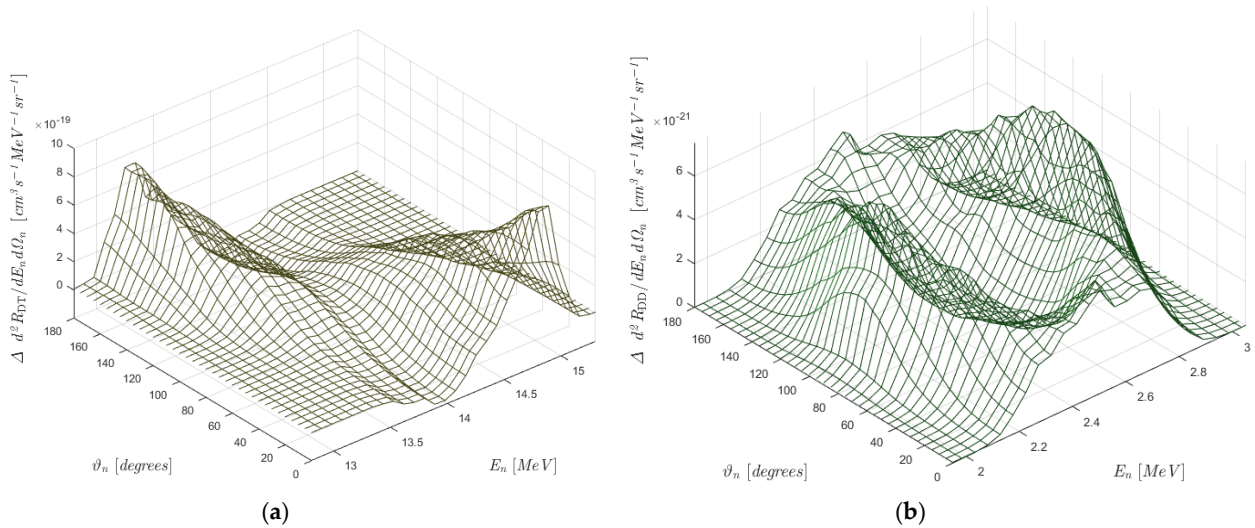


Figure 5. Differences between the distributions of fusion neutrons shown in Figure 4, calculated as the distribution without the speed diffusion effect, subtracted from the corresponding distribution with the speed diffusion effect (a) “blue surface minus grey surface” for ${}^3\text{H}({}^2\text{H},n){}^4\text{He}$ reactions; (b) “blue surface minus grey surface” for ${}^2\text{H}({}^2\text{H},n){}^3\text{He}$ reactions.

Angularly resolved energy spectra of neutrons produced in ${}^3\text{H}({}^2\text{H},n){}^4\text{He}$ reactions and in ${}^2\text{H}({}^2\text{H},n){}^3\text{He}$ reactions are shown in Figure 6a and in Figure 6b, correspondingly, for the cases when calculations were made using the simplified model (2) not taking into account the speed diffusion effect, and using a more sophisticated model (13), taking into account the speed diffusion in velocity space of fuel nuclei. Although noticeable differences in fusion product spectra can be observed, the obtained results demonstrate similar qualitative behaviour.

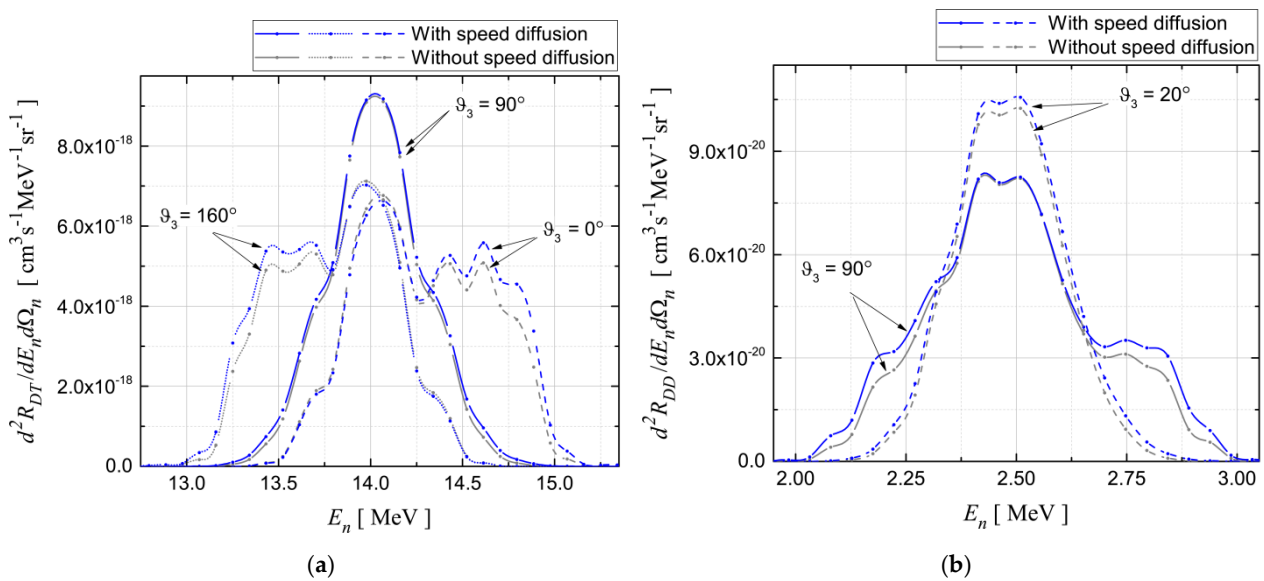


Figure 6. (a) Energy spectra of neutrons produced in ${}^3\text{H}({}^2\text{H},n){}^4\text{He}$ reactions at 0° , 90° , and 160° laboratory frame angles, calculated using velocity distributions of deuterons and tritons shown in Figure 1; (b) energy spectra of neutrons produced in ${}^2\text{H}({}^2\text{H},n){}^3\text{He}$ reactions at 20° and 90° laboratory frame angles, calculated using velocity distributions of deuterons shown in Figure 2.

Total, i.e., integral over the angles, energy spectra of neutrons produced in ${}^3\text{H}({}^2\text{H},\text{n}){}^4\text{He}$ reactions and in ${}^2\text{H}({}^2\text{H},\text{n}){}^3\text{He}$ reactions are shown in Figure 7a and in Figure 7b, correspondingly, for the cases when calculations were made without the speed diffusion effect (dark-blue colour), and with speed diffusion effect (green colour). Integration of the total energy spectra over the entire energy range results in the rate coefficient. The rate coefficient tends to be slightly greater when the speed diffusion is accounted for because of the presence of ions with higher energies in this case.

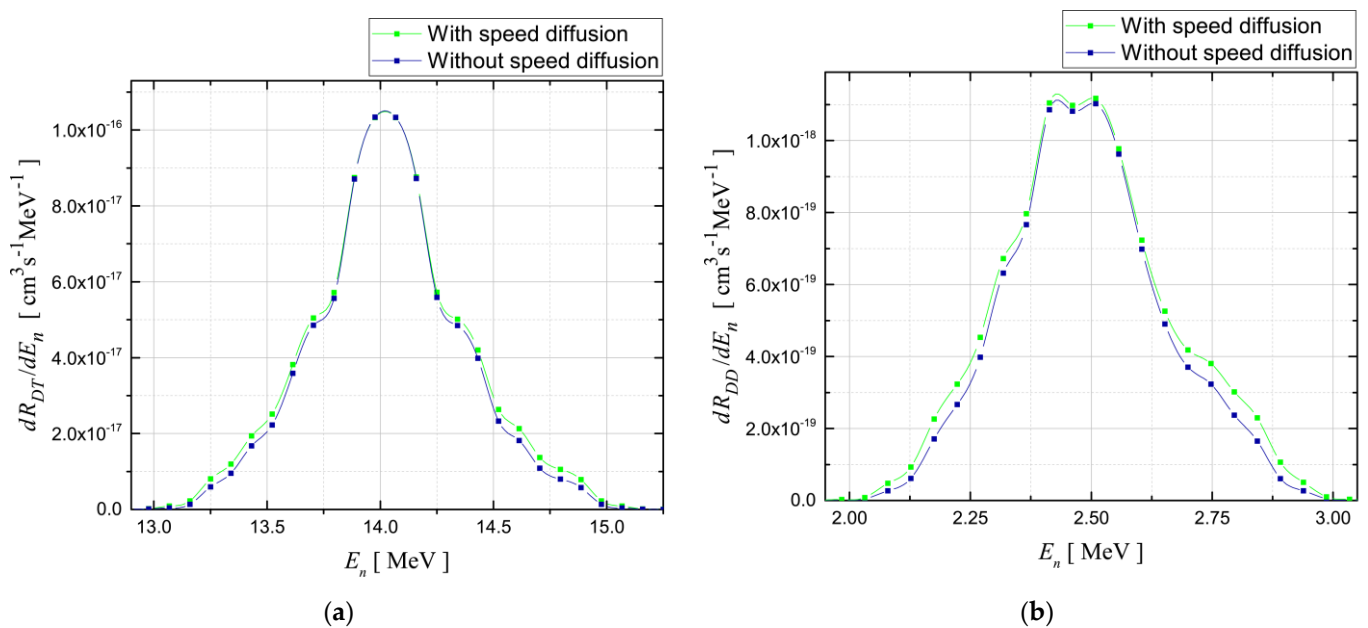


Figure 7. Total energy spectra of neutrons, integrated over the entire range of emission angles, calculated with speed diffusion effect taken into account (green) and without accounting for the speed diffusion effect (dark blue). (a) For ${}^3\text{H}({}^2\text{H},\text{n}){}^4\text{He}$ reactions corresponding to velocity distributions of deuterons and tritons shown in Figure 1; (b) for ${}^2\text{H}({}^2\text{H},\text{n}){}^3\text{He}$ reactions corresponding to velocity distributions of deuterons shown in Figure 2.

Squares in Figures 6 and 7 depict the calculated values for the selected neutron energy grid, while the solid lines depict spline approximations.

4. Conclusions

Calculations of distributions of fusion neutrons in the presence of suprathermal deuterium and tritium nuclei originating from a monoenergetic source in Maxwellian plasma have been performed. The role of the speed diffusion effect in the fuel nuclei velocity space in the formation of energy distributions of products of ${}^3\text{H}({}^2\text{H},\text{n}){}^4\text{He}$ and ${}^2\text{H}({}^2\text{H},\text{n}){}^3\text{He}$ fusion reactions has been studied. High-energy tails of distributions of fast ion velocities in the regions below and above the beam injection velocity influence the energetic and angular distributions of nuclear fusion products.

The effect of the fast ion speed diffusion on the obtained neutron spectra is noticeable; however, it does not significantly modify the qualitative behavior of the spectra and such general parameters as full width at half maximum. Thus, the use of simplified analytical models for the ion distribution functions is reasonably justified when the knowledge of “fine structure” of neutron spectra is not required.

Advanced plasma diagnostics, such as high-resolution neutral particle analysis combined with high-resolution neutron spectrometry, may be used for experimental validation of the mathematical models described herein. Recent progress on the development of active charge exchange diagnostics of fast ion distributions and neutron spectroscopic diagnostics on Globus-M2 spherical tokamak [44] were reported in [45] and [46], respectively. An

excellent powerful set of neutron diagnostics operating on the Large Helical Device (LHD) in combination with advanced diagnostics of energetic ions was described in [47]. Measurements of anisotropic distributions of fusion neutrons in experiments with deuterium plasma heated by neutral beam injection on LHD were reported in [48]. Neutron emission spectroscopy on Joint European Torus (JET) was overviewed in [49]. Prospects of various neutron diagnostics foreseen for ITER, including neutron flux monitors and spectrometers, were described in [50].

The results may be applied for simulations of energetic and angular distributions of neutrons and charged nuclear fusion products in magnetically confined plasma in the framework of the activities on the development of fusion energy reactors and fusion neutron sources employing beam–plasma interactions.

Funding: The research was funded by the Ministry of Science and Higher Education of the Russian Federation under the strategic academic leadership program “Priority 2030” (Agreement 075-15-2021-1333 dated 30.09.2021) and partially supported in the framework of the IAEA Coordinated Research Project under contract No. 22765.

Informed Consent Statement: Not applicable.

Data Availability Statement: Not applicable.

Acknowledgments: The results were obtained using computational resources of Peter the Great Saint Petersburg Polytechnic University’s Supercomputing Center (scc.spbstu.ru).

Conflicts of Interest: The author declares no conflict of interest.

References

1. Goto, T.; Tanaka, T.; Tamura, H.; Miyazawa, J.; Iwamoto, A.; Yanagi, N.; Fujita, T.; Kodama, R.; Mori, Y. Feasibility study of tokamak, helical and laser reactors as affordable fusion volumetric neutron sources. *Nucl. Fusion* **2021**, *61*, 126047. [[CrossRef](#)]
2. Gryaznevich, M.P. Research on fusion neutron sources. *AIP Conf. Proc.* **2012**, *1442*, 55–64. [[CrossRef](#)]
3. Sykes, A.; Gryaznevich, M.P.; Voss, G.; Kingham, D.; Kuteev, B. Fusion for Neutrons: A Realizable Fusion Neutron Source. *IEEE Trans. Plasma Sci.* **2012**, *40*, 715–723. [[CrossRef](#)]
4. Kuteev, B.; Azizov, E.; Bykov, A.; Dnestrovsky, A.; Dokuka, V.; Gladush, G.; Golikov, A.; Goncharov, P.; Gryaznevich, M.P.; Gurevich, M.; et al. Steady-state operation in compact tokamaks with copper coils. *Nucl. Fusion* **2011**, *51*, 073013. [[CrossRef](#)]
5. Shpanskiy, Y.S.; DEMO-FNS Project Team. Progress in the design of the DEMO-FNS hybrid facility. *Nucl. Fusion* **2019**, *59*, 076014. [[CrossRef](#)]
6. Sakai, R.; Fujita, T.; Okamoto, A. Economy of Tokamak Neutron Source for Transmutation of Transuranics. *Plasma Fusion Res.* **2019**, *14*, 1405040. [[CrossRef](#)]
7. Chirkov, A.Y.; Fedyunin, D.E. On the feasibility of fusion–fission hybrid based on deuterium fuelled tokamak. *Fusion Eng. Des.* **2019**, *148*, 111302. [[CrossRef](#)]
8. Stacey, W.M. Tokamak D–T fusion neutron source requirements for closing the nuclear fuel cycle. *Nucl. Fusion* **2007**, *47*, 217–221. [[CrossRef](#)]
9. Štancar, Ž.; Gorelenkova, M.; Conroy, S.; Sauvan, P.; Buchanan, J.; Weisen, H.; Snoj, L.; Contributors, J. Multiphysics approach to plasma neutron source modelling at the JET tokamak. *Nucl. Fusion* **2019**, *59*, 096020. [[CrossRef](#)]
10. Salazar-Cravioto, H.; Nieto-Perez, M.; Ramos, G.; Mahajan, S.; Valanju, P.; Kotschenreuther, M. Modeling of a Spherical Tokamak as an Extended Neutron Source Using ASTRA and MCNP. *IEEE Trans. Plasma Sci.* **2020**, *48*, 1810–1816. [[CrossRef](#)]
11. Zhirkin, A.V.; Kuteev, B.V. Three-dimensional model of DEMO-FNS facility considering neutronics and radiation shield problems. *Heliyon* **2019**, *5*, E01630. [[CrossRef](#)] [[PubMed](#)]
12. Ericsson, G. Advanced Neutron Spectroscopy in Fusion Research. *J. Fusion Energy* **2019**, *38*, 330–355. [[CrossRef](#)]
13. Sugiyama, S.; Matsuura, H.; Uchiyama, D. Incident neutron spectra on the first wall and their application to energetic ion diagnostics in beam-injected deuterium–tritium tokamak plasmas. *Phys. Plasmas* **2017**, *24*, 092517. [[CrossRef](#)]
14. Sugiyama, S.; Matsuura, H. Modification of neutron emission spectrum by Alfvén eigenmodes in a deuterium–tritium plasma. *Fusion Eng. Des.* **2019**, *146*, 320–324. [[CrossRef](#)]
15. Abdou, M.; Morley, N.B.; Smolentsev, S.; Ying, A.; Malang, S.; Rowcliffe, A.; Ulrickson, M. Blanket/first wall challenges and required R&D on the pathway to DEMO. *Fusion Eng. Des.* **2015**, *100*, 2–43. [[CrossRef](#)]
16. Titarenko, Y.E.; Batyaev, V.; Pavlov, K.V.; Titarenko, A.Y.; Alekseev, P.N.; Gurevich, M.I.; Dudnikov, A.A.; Zhirkin, A.V.; Kuteev, B.; Koldobskii, A.B.; et al. Benchmark Experiments for Verifying the Working Parameters of the Blankets of a Thermonuclear Neutron Source. *At. Energy* **2016**, *120*, 55–62. [[CrossRef](#)]
17. Zhou, Z.; Yang, Y.; Xu, H. Study on fission blanket fuel cycling of a fusion–fission hybrid energy generation system. *Nucl. Fusion* **2011**, *51*, 103011. [[CrossRef](#)]

18. Zhirkin, A.; Kuteev, B.; Gurevich, M.; Chukbar, B. Neutronics analysis of blankets for a hybrid fusion neutron source. *Nucl. Fusion* **2015**, *55*, 113007. [CrossRef]
19. Kuteev, B.V.; Goncharov, P.R. Fusion–Fission Hybrid Systems: Yesterday, Today, and Tomorrow. *Fusion Sci. Technol.* **2020**, *76*, 836–847. [CrossRef]
20. Kuteev, B.V.; Shpanskiy, Y.S. Fusion-fission hybrid system development and integration into Russia’s nuclear power engineering. *Probl. At. Sci. Technol. Ser. Thermonucl. Fusion* **2021**, *44*, 836–847. [CrossRef]
21. Almagambetov, A.N.; Chirkov, A.Y. Power and Sizes of Tokamak Fusion Neutron Sources with NBI-Enhanced Reaction Rate. *J. Fusion Energ.* **2016**, *35*, 841–848. [CrossRef]
22. Dlougach, E.; Shlenskii, M.; Kuteev, B. Neutral Beams for Neutron Generation in Fusion Neutron Sources. *Atoms* **2022**, *10*, 143. [CrossRef]
23. Štancar, Ž. Generation of a plasma neutron source for Monte Carlo neutron transport calculations in the tokamak JET. *Fusion Eng. Des.* **2018**, *136*, 1047–1051. [CrossRef]
24. Sirén, P.; Varje, J.; Äkäslompolo, S.; Asunta, O.; Giroud, C.; Kurki-Suonio, T.; Weisen, H.; Contributors, T.J. Versatile fusion source integrator AFSI for fast ion and neutron studies in fusion devices. *Nucl. Fusion* **2018**, *58*, 016023. [CrossRef]
25. Goncharov, P.R. Spectra of neutrons from a beam-driven fusion source. *Nucl. Fusion* **2015**, *55*, 063012. [CrossRef]
26. Goncharov, P.R. Reduction of the isotropic S-formula for the energy spectrum of nuclear fusion products to a triple integral. *Plasma Phys. Control. Fusion* **2020**, *62*, 072001. [CrossRef]
27. Goncharov, P.R.; Bakharev, N.N. Anisotropic distributions of deuterium–deuterium nuclear fusion products in a compact tokamak. *Plasma Phys. Control. Fusion* **2020**, *62*, 125016. [CrossRef]
28. Lehner, G.; Pohl, F. Reaktionsneutronen als Hilfsmittel der Plasmadiagnostik. *Z. Phys.* **1967**, *207*, 83–104. [CrossRef]
29. Lessor, D.L. *Neutron and Alpha Particle Energy Spectrum and Angular Distribution Effects from Beam-Plasma D-T Fusion*; Rept. BNWL-B-409; Battelle Pacific Northwest Labs.: Richland, WA, USA, 1975.
30. Towner, H.H.; Jassby, D.L. Energy Spectra of Fusion Neutrons from Plasmas Driven by Reacting Ion Beams. In Proceedings of the Winter Meeting of the American Nuclear Society, San Francisco, CA, USA, 16 November 1975.
31. Källne, J.; Ballabio, L.; Frenje, J.; Conroy, S.; Ericsson, G.; Tardocchi, M.; Traneus, E.; Gorini, G. Observation of the Alpha Particle “Knock-On” Neutron Emission from Magnetically Confined DT Fusion Plasmas. *Phys. Rev. Lett.* **2000**, *85*, 1246–1249. [CrossRef]
32. Matsuura, H.; Nakao, Y. Modification of alpha-particle emission spectrum in beam-injected deuterium-tritium plasmas. *Phys. Plasmas* **2009**, *16*, 042507. [CrossRef]
33. Scheffel, J. Neutron spectra from beam-heated fusion plasmas. *Nucl. Instr. Methods Phys. Res.* **1984**, *224*, 519–531. [CrossRef]
34. Eriksson, J.; Conroy, S.; Sundén, E.A.; Hellesen, C. Calculating fusion neutron energy spectra from arbitrary reactant distributions. *Comput. Phys. Commun.* **2016**, *199*, 40–46. [CrossRef]
35. Abe, Y.; Johzaki, T.; Sunahara, A.; Arikawa, Y.; Ozaki, T.; Ishii, K.; Hanayama, R.; Okihara, S.; Miura, E.; Komeda, O.; et al. Monte Carlo particle collision model for qualitative analysis of neutron energy spectra from anisotropic inertial confinement fusion. *High Energy Density Phys.* **2020**, *36*, 100803. [CrossRef]
36. Heidbrink, W.W. Analytical expressions for fusion spectra produced in “beam-target” fusion reactions. *Rev. Sci. Instrum.* **1985**, *56*, 1098–1099. [CrossRef]
37. Appelbe, B.; Chittenden, J. The production spectrum in fusion plasmas. *Plasma Phys. Control. Fusion* **2011**, *53*, 045002. [CrossRef]
38. Tiesinga, E.; Mohr, P.J.; Newell, D.B.; Taylor, B.N. CODATA recommended values of the fundamental physical constants: 2018. *Rev. Mod. Phys.* **2021**, *93*, 025010. [CrossRef]
39. Goncharov, P.; Kuteev, B.; Ozaki, T.; Sudo, S. Analytical and semianalytical solutions to the kinetic equation with Coulomb collision term and a monoenergetic source function. *Phys. Plasmas* **2010**, *17*, 112313. [CrossRef]
40. Drosig, M.; Otuka, N. International Nuclear Data Committee Report INDC(AUS)-0019, 2019, IAEA Nuclear Data Section. Available online: <https://www-nds.iaea.org/publications/indc/indc-aus-0019.pdf> (accessed on 5 January 2023).
41. Goncharov, P.R. Differential and total cross sections and astrophysical S-factors for ${}^2\text{H}(d,n){}^3\text{He}$ and ${}^2\text{H}(d,p){}^3\text{H}$ reactions in a wide energy range. *At. Data Nucl. Data Tables* **2018**, *120*, 121–151. [CrossRef]
42. Dnestrovskiy, A.Y.; Goncharov, P.R. Numerical and semi-analytical treatments of neutral beam current drive in DEMO-FNS. *Fusion Eng. Des.* **2017**, *123*, 440–443. [CrossRef]
43. Goncharov, P.R. Analytical and statistical modelling of the fast ion source due to neutral beam injection in magnetically confined plasma. *Atoms*, 2023; submitted.
44. Petrov, Y.; Gusev, V.K.; Sakharov, N.; Minaev, V.; Varfolomeev, V.; Dyachenko, V.; Balachenkov, I.M.; Bakharev, N.N.; Bondarchuk, E.N.; Bulanin, V.; et al. Overview of GLOBUS-M2 spherical tokamak results at the enhanced values of magnetic field and plasma current. *Nucl. Fusion* **2022**, *62*, 042009. [CrossRef]
45. Bakharev, N.N.; Balachenkov, I.M.; Chernyshev, F.V.; Gusev, V.K.; Kiselev, E.; Kurskiev, G.S.; Melnik, A.D.; Minaev, V.; Mironov, I.M.; Nesenevich, V.; et al. Measurement of the fast ion distribution using active NPA diagnostics at the Globus-M2 spherical tokamak. *Plasma Phys. Control. Fusion* **2021**, *63*, 125036. [CrossRef]
46. Iliasova, M.; Shevelev, A.; Khilkevitch, E.; Bakharev, N.; Skrekel, O.; Minaev, V.; Doinikov, D.; Gin, D.; Gusev, V.; Kornev, V.; et al. Neutron diagnostic system at the Globus-M2 tokamak. *Nucl. Instrum. Methods Phys. Res. A* **2022**, *1029*, 166425. [CrossRef]
47. Isobe, M.; Ogawa, K.; Sangaroon, S.; Kamio, S.; Fujiwara, Y.; Osakabe, M. Recent development of neutron and energetic-particle diagnostics for LHD deuterium discharges. *JINST* **2022**, *17*, C03036. [CrossRef]

48. Sugiyama, S.; Nishitani, T.; Matsuura, H.; Isobe, M.; Ogawa, K.; Tanaka, T.; Yoshihashi, S.; Uritani, A.; Osakabe, M. Observation of neutron emission anisotropy by neutron activation measurement in beam-injected LHD deuterium plasmas. *Nucl. Fusion* **2020**, *60*, 076017. [[CrossRef](#)]
49. Giacomelli, L.; Hjalmarsson, A.; Sjöstrand, H.; Glasser, W.; Källne, J.; Conroy, S.; Ericsson, G.; Johnson, M.G.; Gorini, G.; Henriksson, H.; et al. Advanced neutron diagnostics for JET and ITER fusion experiments. *Nucl. Fusion* **2005**, *45*, 1191. [[CrossRef](#)]
50. Bertalot, L.; Krasilnikov, V.; Core, L.; Saxena, A.; Yukhnov, N.; Barnsley, R.; Walsh, M. Present Status of ITER Neutron Diagnostics Development. *J. Fusion Energy* **2019**, *38*, 283. [[CrossRef](#)]

Disclaimer/Publisher's Note: The statements, opinions and data contained in all publications are solely those of the individual author(s) and contributor(s) and not of MDPI and/or the editor(s). MDPI and/or the editor(s) disclaim responsibility for any injury to people or property resulting from any ideas, methods, instructions or products referred to in the content.